TIME-DOMAIN DEMODULATION OF RHESSI LIGHT CURVES

KASPAR ARZNER
Paul Scherrer Institut, CH-5232 Villigen PSI, Switzerland

(Received 5 August 2002; accepted 11 September 2002)

Abstract. This paper presents an algorithm to decompose the modulated RHESSI light curves into periodic functions and a smooth function, representing the true (demodulated) time profile of an impulsive source. The decomposition is achieved by optimizing a trade-off between the Poisson likelihood, a smoothness constraint, and conditions on the average grid transmission and the (modulating or non-modulating) background. The algorithm, which operates on the level of count rates and does not require imaging information, is verified by numerical simulations and applied to some early RHESSI data, where – as a preliminary result – several impulsive features on time scales < 4 s may have been identified.

1. Introduction

The RHESSI instrument uses the rotational modulation principle in combination with germanium detectors to obtain spatially, spectrally, and temporally resolved images of solar HXR outbursts. The interpretation of the observed counts raises a series of inverse problems, such as the deconvolution of the spectral response (Smith *et al.*, 2002), and the image reconstruction from the modulated count rates (Hurford *et al.*, 2002). In this article, the focus is on the 'reverse' problem, i.e., on the estimation of the true time dependence of the source on time scales below the RHESSI spin period $T_s \sim 4$ s. The motivation for this stems from earlier HXR observations, which revealed impulsive features on sub-second time scales in some 10% of all flares with sufficient count rates to see such variations (Dennis, 1985). The shortest features found so far were called 'HXR spikes'; they have typical durations of order of 400 ms (Kiplinger *et al.* (1984) from HXRB/SMM; Machado *et al.* (1993) from BATSE/CGRO), and rise times in the order of $\tau_s \sim 100$ ms; occasionally, even shorter time scales of a few 10 ms have been observed (see Dennis, 1985). The sub-second evolution of the HXR light curves is believed to be in close relation with the energy release process, and is therefore interesting from an acceleration physics point of view (Benz *et al.*, 1994; Miller *et al.*, 1997), and relevant for the comparison with radio data (e.g., Gary, 2000; Nakajima, 2000).

The modulational contributions can be eliminated by different methods such as non-recursive (time-domain) filters ($O_n = \sum_{i<n} a_i I_i$ with I the input and O the output signals), recursive filters ($O_n = \sum_{i<n} a_i O_i + \sum_{j\le n} b_j I_j$), autoregressive models (e.g., Rosen and Porat, 1989), or (frequency-domain) Wiener filters (Kailath, 1974; Mallat, 1998). The latter option has been closely examined, and a

Solar Physics **210:** 213–227, 2002.

demodulation method based on it will be presented in a separate communication. The classical Wiener filter minimizes the deviation of the restored and true signals on the basis of the power spectral densities of the signal and noise.

Singular spectrum analysis (SSA) (Vautard and Ghil, 1989; Varadi *et al.*, 1999, 2000) offers another, more general, approach to the detection of periodic structures in noisy data. SSA disentangles deterministic (periodic or chaotic) and stochastic contributions of an observed time series, and identifies the dimension of an underlying dynamical system. This is achieved by considering the singular values of the covariance of vectors of consecutive (or time-ordered) observations, with the motivation that a single differential equation of order d (involving d discrete values) is equivalent to a d-dimensional system of first-order equations. SSA does not require an independent estimate on the period of the deterministic contribution, and could therefore apply to situations where the RHESSI spin period is unknown. In what follows, however, we focus on the (usual) case where T_S is known.

The modulation involves two time scales. The first one is the fine-scale modulation which would result from a pair of well separated grids ('modulation amplitude'), and the second one is the slower modulation due to the internal shadowing of each individual grid ('grid transmission'). Together, these modulational contributions yield a 'chirp' covering the frequency range from ~ 1 Hz up to $k^i \rho / T_S$ Hz, with $k^i = 2\pi / p^i$ the wave vector of the ith subcollimator i (p^i being its angular pitch), and ρ the distance between the imaging axis and the source(s). As a consequence of their broad-band nature, the modulation frequencies tend to interfere with the signal frequencies, and a proper separation requires the inclusion of phase information into the Wiener filter, or the use of non-uniform representations such as Bessel functions or wavelets (Mallat, 1998). This insight is consolidated if one keeps in mind that the modulation is deterministic rather than stochastic. However, phase information requires a preceding estimate of the source position(s) or an equivalent phase identification from the count rates, and thus a higher level of pre-processing. A similar caveat holds for non-recursive (time domain) filters, which are equivalent to convolutions. In order to effectively suppress spin period artifacts the convolution kernel must decay on a time scale $> T_S$, which yields an undesirably vigorous smoothing of the demodulated signal.

When the RHESSI subcollimators sweep an unknown brightness distribution they create, in general, a light curve of complex shape. However, one statement can be made without any detailed knowledge of the brightness distribution: the observed intensities must be T_S-periodic if precession and angular acceleration can be neglected, and if the source distribution did not change with time. An intuitive way to see this projects the transmission probability to the solar disk ('modulation pattern') (Figure 1). In the absence of precession, the rotation axis remains stationary, and the imaging (optical) axis $\mathbf{P}(t)$ (dotted circle) rotates around the rotation axis with rigidly co-rotating wave vector $\mathbf{k}(t)$ of the subcollimator (Figure 1 top). By convention, $\mathbf{P}(t)$ is measured with respect to the Sun center (Fivian *et al.*, 2002). The angle between the imaging axis and the rotation axis is called the

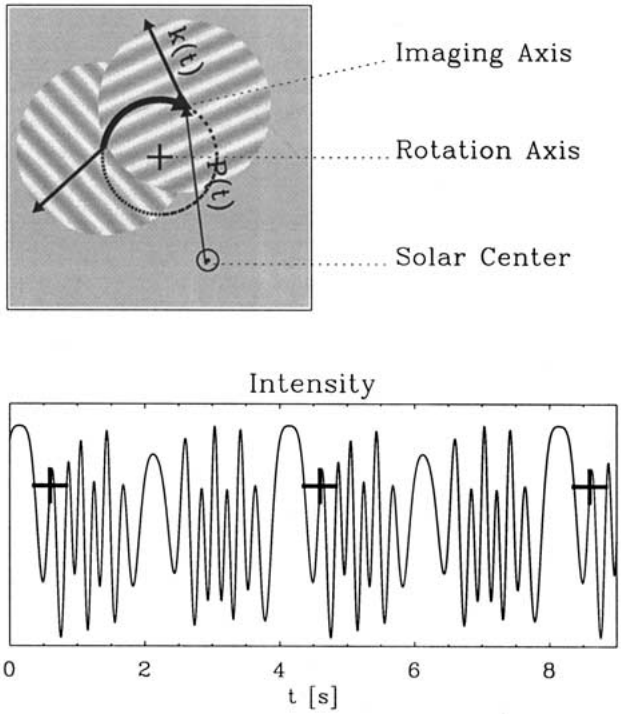

Figure 1. Illustration of the rotational modulation in the absence of precession but presence of coning. *Top panel*: in the inertial (solar) frame, the imaging axis $\mathbf{P}(t)$ rotates clockwise around the rotation axis, and carries rigidly along the subcollimator's wave vector $\mathbf{k}(t)$. Two subsequent snapshots are shown. If the solar brightness distribution is time-independent, then the observed light curve is periodic with the RHESSI spin period $T_S \sim 4$ s (*bottom*: crosses denote sample intensities for better clarity.)

coning angle, and RHESSI is 'coning' if this angle is different from zero. Clearly, the modulation pattern reproduces itself after T_S (and possibly also after $nT_S/2$ for favourable $\mathbf{P}(nT_S/2)$), implying equal Poisson intensities for a stationary (or T_S-periodic) brightness distribution. This fact is exploited by the demodulation method proposed in the present paper. The method essentially detects deviations from periodicity, and assigns them to the intrinsic time dependence of the source distribution. It is thus limited to time intervals with a (relatively) stable spin axis.

The organization is as follows: Section 2 outlines the modulation principle, Section 3 defines the demodulation (inverse) method, Section 4 describes numerical issues and tests, Section 5 shows some examples of early RHESSI data, and Section 6 contains a brief discussion and preliminary conclusions.

2. Forward Model

The method invokes the following assumptions on the ordering of relevant time scales. First, the time τ_b over which the solar (gradual flare) and non-solar (cosmic, magnetospheric) backgrounds can be considered as constant satisfies $\tau_b \gg T_S$, where τ_b is of the order of a minute. This rules out, for instance, times just before South Atlantic Anomaly crossings. Secondly, the RHESSI spin period can be considered as constant during τ_b. The source variability itself, as outlined above, is expected to involve time scales down to $\tau_s \sim 100$ ms. Throughout this paper, the analysis is restricted to time intervals of duration $\leq \tau_b$, and to a fixed energy band which is the same for all subcollimators.

The photons arriving at detector i are supposed to be Poisson distributed with time-dependent intensities $\lambda^i(t) = \int M^i(\mathbf{x}, t)\, B(\mathbf{x}, t)\, \mathrm{d}\mathbf{x}$, where $\mathbf{x}$ are coordinates in the (solar) image plane, $M^i(\mathbf{x}, t)$ is the ith modulation pattern, and $B(\mathbf{x}, t)$ is the brightness distribution, which, during τ_b, is modeled as $B(\mathbf{x}, t) = B_0(\mathbf{x}) + B_1(\mathbf{x}, t)$. Here, $B_1(\mathbf{x}, t)$ represents an 'impulsive' source and $B_0(\mathbf{x})$ is a stationary background. The short rise time of HRX spikes indicates a – presumably unique – compact source ($c\tau_s \lesssim 1'$ by causality; $v_\mathrm{A}\tau_s < 1''$ by the Alfvén travel time), so that one may set $B_1(\mathbf{x}, t) = s(t)B_1(\mathbf{x})$ with some localized function $B_1(\mathbf{x})$ and $s(t)$ the true time profile. The temporal modulation due to a point source located at $\mathbf{x}_s$, $M^i(t) = \int M^i(\mathbf{x}, t)\delta(\mathbf{x} - \mathbf{x}_s)\, \mathrm{d}\mathbf{x}$, is called the 'modulation function'. Its average over time and over the RHESSI field of view is denoted by a_0^i ($\sim$ average grid transmission), and the fundamental Fourier coefficient of $M^i(t)$ is denoted by a_1^i ($\sim$ modulation amplitude). These quantities are taken from the grid transmission software (Hurford *et al.*, 2002b)

Under the above assumptions, the Poisson intensities have the form $\lambda^i(t) = b^i(t) + m^i(t)s(t)$, with an arbitrary positive function $s(t)$, and where the functions $b^i(t)$ and $m^i(t)$ are positive and T_S-periodic (including the constant case). The functions $s(t)$, $m^i(t)$ and $b^i(t)$ represent the true time profile, the modulation, and the background, respectively. More precisely, the functions $b^i(t)$ and $m^i(t)$ return to comparable values at times $\{t\}$ with comparable aspect data, in the sense that

$$\left(\frac{\pi a_1^i}{p^i}\right)^2 \left\langle r_\odot^2(\Phi(t) - \langle\Phi\rangle)^2 + |\mathbf{P}(t) - \langle\mathbf{P}\rangle|^2 \right\rangle < \epsilon^2\,, \tag{1}$$

where $\Phi(t)$ is the roll angle, $\mathbf{P}(t)$ is the imaging axis in heliocentric coordinates (Figure 1), $r_\odot$ is the solar radius, and averages are over the time set $\{t\}$. Equation (1) is a sufficient (but not necessary) condition for the rms deviation of the modulation functions being less than ϵ, under the 'worst-case' assumption that the distance between the imaging axis and the source is one solar radius. In practice, $\epsilon < 0.1\, a_0^i$ is found to suppress artifacts due to violation of the periodicity assumption. On times scales $\lesssim 10\, T_S$ and for the coarser grids, Equation (1) is dominated by $\Phi(t)$, whereas on longer terms, the non-recurrent motion of $\mathbf{P}(t)$ cuts off the comparable times. This long-term cut off varies widely from orbit to orbit, and may completely

inhibit periodicity for the finest subcollimators. It is assumed that for times satisfying Equation (1), and within the accuracy required by Equation (1), $\Phi(t)$ can be replaced by a linear function of time. This reduces the aspect recurrence to time periodicity, and admits a simple numerical implementation. The roll angle is taken from the PMTRAS instrument (Hurford and Curtis, 2002), with a relative (period-to-period) angular accuracy of $\sim 1'$. The imaging axis is provided by the SAS instrument (Fivian *et al.*, 2002), the accuracy of which is $\Delta\mathbf{P} < 1''$. The term $b^i(t)$ also accounts for a time-independent non-solar background, which – as long as it passes the RHESSI detectors – is T_S-periodic.

Soon after the RHESSI launch it became evident that the observed count rates suffer from so-called dropouts where the count rate is zero (Smith *et al.*, 2002; Schwartz *et al.*, 2002). The dropouts are presumably due to cosmic rays hitting the detectors. Empirically, they occur at random with frequency ~ 1 Hz and exponentially distributed durations of decay time ~ 0.25 s, as if they were triggered and terminated by subsequent points of a Poisson process of intensity ~ 4 Hz. The dropouts, together with the detector dead time, are unified in a lifetime flag L_k^i (Schwartz *et al.*, 2002), which measures the fraction of operational time in each time bin (i.e., $L_k^i = 0.8$ indicates that detector i was operational during 80 percent of the time interval $t_k \ldots t_{k+1}$). For the present purpose, count rates with $L_k^i < 0.5$ are ignored, and corrected for lifetime if $0.5 < L_k^i < 1$.

3. Demodulation

Consider a time interval τ_b with the count rates binned at an integer factor of the spin period, or at a sufficient number of spacecraft binary μs bins, such that round off does not affect Equation (1). Since $\tau_b > T_S$, this requires somewhat finer time bins (Δt) than the SSW default. Assume that the corresponding discrete times satisfy Equation (1). The forward model for the count rates is then

$$\lambda_t^i = b^i_{(t \bmod N_S)} + r_t \, m^i_{(t \bmod N_S)} , \tag{2}$$

where $N_S = T_S/\Delta t$, r_t is the retrieved 'impulsive' time profile (the estimate for $s(t)$), and we have adopted the convention that superscripts label subcollimators, and subscripts label time. Clearly, the decomposition with Equation (2) is ill-posed or ill-conditioned. A unique solution may, however, be found by assigning as much time variation to modulation as possible. To this end, the goal function

$$F = \underbrace{\sum_{i,j,k}^{*} \left\{ -(b^i_j + m^i_j r_{j+N_S k}) + c^i_{j+N_S k} \left(1 + \ln \frac{b^i_j + m^i_j r_{j+N_S k}}{c^i_{j+N_S k}} \right) \right\}}_{\ln L/L_0} - \\ - \underbrace{\frac{\alpha}{2} \sum_t (r_{t+1} - r_t)^2}_{A} - \underbrace{\frac{\beta}{2} \sum_i \left(a^i_0 - \frac{1}{P} \sum_j m^i_j \right)^2}_{B} + \underbrace{\gamma \sum_{i,j} \ln b^i_j}_{C} \tag{3}$$

is maximized with respect to r, m and b (omitted indices indicate the full index set). Above, c stands for the observed count rates, and α, β, γ are positive numbers defined below. The different terms in Equation (3) represent different design goals of the demodulation algorithm. The first term is the Poisson maximum log likelihood ratio, which reduces to minus one half times the usual chi square expression in the limit of large count rates (Eadie *et al.*, 1971; Cash, 1979). The asterisk indicates that the sum is restricted to valid times and subcollimators (no dropouts) and that the lifetime correction is applied if necessary. The second term (A) represents a smoothness constraint for minimum derivatives; if data are lacking (dropouts), this term attempts to linearly interpolate r across the data gap. The third term (B) ties down the mean values $\langle m^i \rangle$, which are relatively insensitive to the exact source shape and -position (except for spin axis artifacts in the absence of coning), and can be predicted from the grid geometry alone. The fourth term (C), finally, resolves the overall ambiguity between b and mr in favour of b, such as that periodic contributions from a constant offset of $s(t)$ are attributed to the background, and m (and hence r) is not contaminated by b. In a Bayesian (Eadie *et al.*, 1971) interpretation, $(C - A - B)$ is proportional to the logarithm of the a priori probability of (r, m, b).

Numerical experience shows, and analytical arguments (Appendix) support, that Equation (3) has a unique solution (global maximum) for sufficiently large α, β, γ. The current choice is as follows. First, $\alpha = N N_t^{-1} (\tau^2/\Delta t)^2 \bar{r}^{-1}$ with N the number of valid count rates, N_t the number of time bins, $\bar{r} = \sum^*_{it} c^i_t / \sum^*_{it} a^i_0$, and 0.1 s $< \tau <$ 1 s. This allows r to vary by $\sim \sqrt{\bar{r}}$ over the *a priori correlation time* τ. The second regularization parameter is $\beta = N N_c^{-1} (0.2\, a_0)^{-2}$ with N_c the number of subcollimators, which admits a 20% deviation of the retrieved versus theoretical average grid transmissions. The third parameter is $\gamma \lesssim \frac{1}{2} N/(P N_c \ln \bar{c})$ with the average observed (valid) count rate. The upper limit for γ is needed in the presence of a dominant background; otherwise, γ may be smaller without losing its regularizing function.

At low count rates (< 1000 counts s^{-1} subcollimator^{-1}), there may not be enough information available to reliably determine the full model $b + mr$. In this situation, the background degrees of freedom are 'frozen in' ($b^i_t = 0$). This applies especially to energies above 20 keV, whereas the full model becomes important at energies ~ 10 keV with significant background contribution. Note that a frozen background still allows for a *constant* offset, $\lambda^i_t = b^i_0 + m^i_t s_t$, which is included in the periodic

functions m_t^i and the constant part of s_t. The retrieved and true time profiles are then connected by $r_t = s_t + \sum_i b_0^i / \sum_i a_0^i$.

4. Numerical Tests

Equation (3) is solved in an iterative way. The state vector (r, m, b) is updated by a simplified Newton/Marquardt method (Press *et al.*, 1998) with the Hessian approximated by its diagonal. The diffusion equation resulting from the 'A' term is treated by an implicit (Crank–Nicholson) scheme. The range of m, which is given by the slit-to-slot ratio of the grids, is enforced rigorously in the numerical code, and r and b are enforced to be positive. The initial guess for m_j^i is a_0^i. If b is frozen to zero then the initial guess for r is $r_t = \bar{r}$; otherwise, the initial guesses for r and b are $r_t = \bar{r}/2$ and $b_j^i = \bar{c}/2$. If b is frozen to zero then convergence is reached after some 30 iterations; if b is varied as well, then convergence is somewhat slower.

The algorithm has been tested by numerical simulations with known modulation functions, 'impulsive' time profiles, and backgrounds. A general example is shown in Figure 2. The true brightness distribution is of the form $B(\mathbf{x}, t) = B_0(\mathbf{x}) + s(t)B_1(\mathbf{x})$, where $B_1(\mathbf{x})$ is a point source 0.75 $r_\odot$ away from the imaging axis, and $B_0(\mathbf{x})$ is an extended (200″) stationary source at distance 0.3 $r_\odot$. The imaging axis is assumed to be constant (no coning), and the sources are not aligned with the imaging axis. The modulation functions involve the first harmonics only. The time profile $s(t)$ of the 'impulsive' source (Figure 2 top middle) consists of a linear rise with a superimposed 'spike' at $t = 30$ s. Both the impulsive and stationary sources contribute about the same number of photons, so that the total average count rate is 1600 counts/s/subcollimator, simulated dropouts being included. The simulation involves the subcollimators 7–9. The spin period is 4 s, the time bin size is 8 ms, the total time interval is 1 min, and an error of 0.5% has been added to the spin period in order to account for uncertainties and binning effects. The a priori correlation time of the retrieved signal is $\tau = 0.3$ s. The input to the demodulation algorithm is the Poisson distributed count rates c (Figure 2, left column). Its output is the decomposition into the 'impulsive' time profile r (top left), the functions m (middle column, black: retrieved, gray: true), and the background b (right column, black: retrieved, gray: true). Since the 'impulsive' source is pointlike, m must coincide with the true modulation functions. As can be noticed, the 'spike' is correctly recovered, although its presence might not be obvious from the count rates by eye. Owing to the term (C) in Equation (3), the constant offset of $s(t)$ is (partially) shifted to the background. The numerical convergence is demonstrated in the top right panel, showing the evolution of the figures of merit $\ln L$, A, B, and C as a function of the iteration step. All figures of merit are normalized to the number of valid count rates. In the example of Figure 2, the final reduced log likelihood indicates slight over-resolution, which is tolerated for illustration purposes.

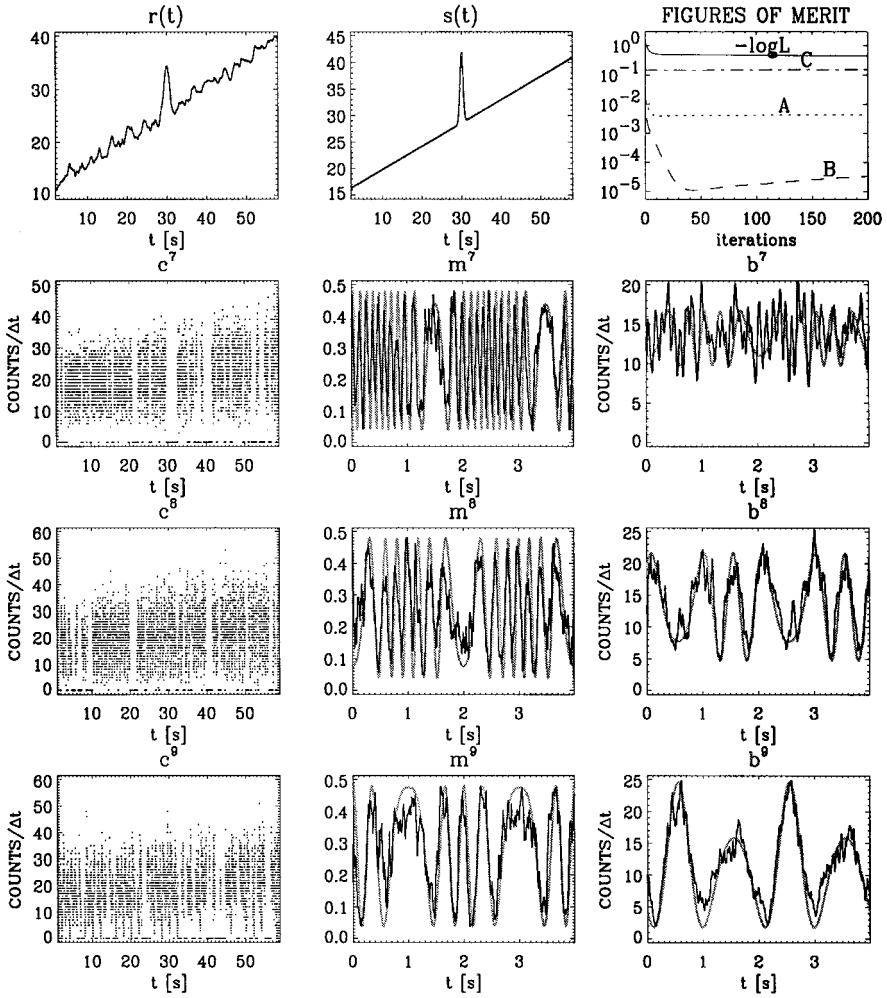

Figure 2. Computer simulation of the demodulation problem. *Top line*: retrieved ($r(t)$) and true ($s(t)$) time profiles, and the figures of merit of Equation (3). *Lines 2 to 4*: simulated counts (*left column*); retrieved/true modulation functions (*middle column, black/gray*); retrieved/true backgrounds (*right column, black/gray*). The time bin size is $\Delta t = 8$ ms, and the *a priori* correlation time is $\tau = 0.3$ s.

5. First Results

After testing with the simulated time series, the demodulation algorithm was applied to several flares observed by RHESSI. A prominent one is the flare of 20 February 2002, 09:58 UT (Figure 3), which is distinguished by both a high peak count rate (~ 6000 counts s^{-1} subcollimator^{-1} in the energy band 12–25 keV) and by a high stability of the spin axis. The motion of the imaging axis $\mathbf{P}(t)$ (Figure 3 middle top) reveals coning but only marginal precession; it is recurrent to better than 10 arc sec over one minute around peak time ($\sim$ 09:58:00 UT). The stability of

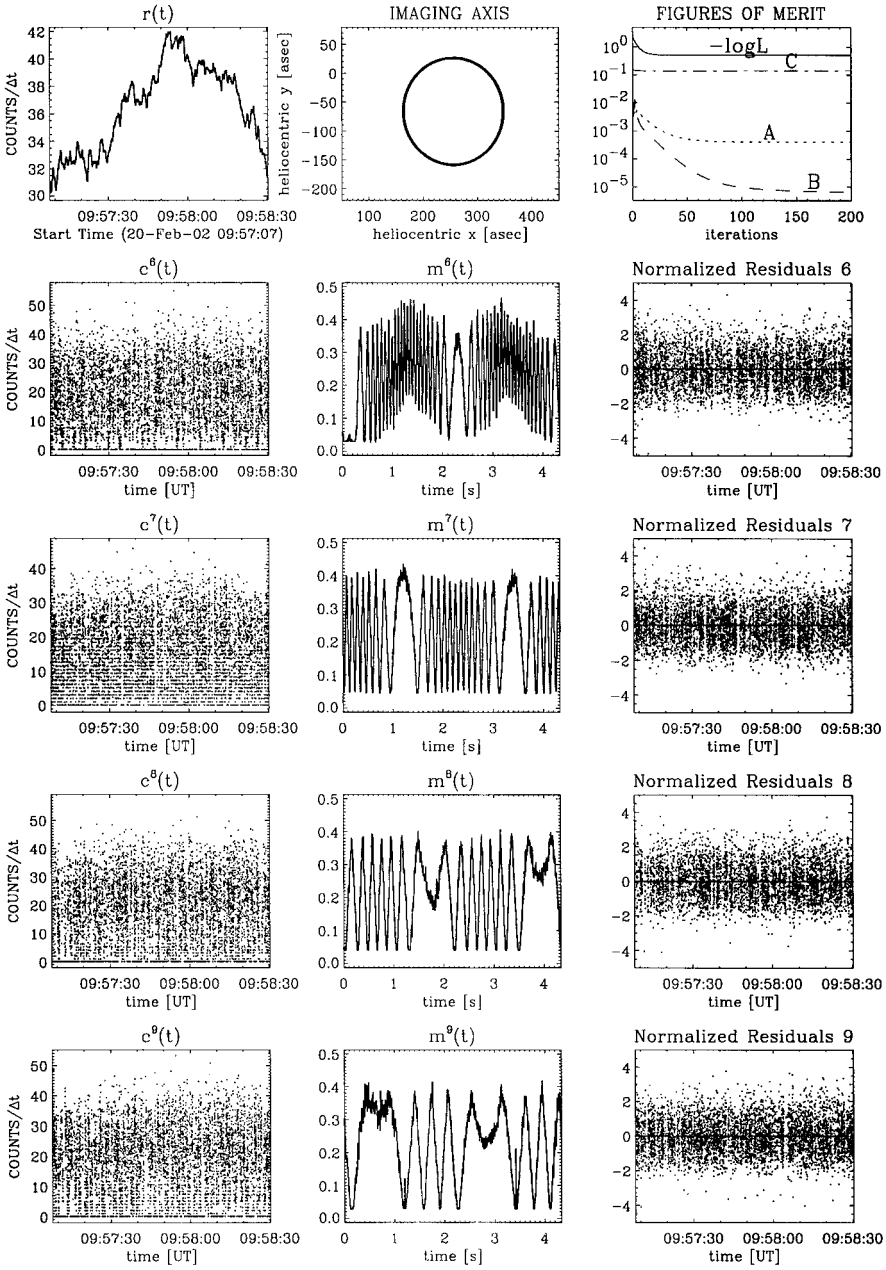

Figure 3. Demodulation of the flare of 20 February 2002, 11:06 UT in the energy band 12–50 keV. The time bin size is $\Delta t = 1.9$ ms and the *a priori* autocorrelation time is $\tau = 0.3$ s. Both the retrieved 'impulsive' time profile (*top left*) and an estimate for the functions m (*middle column*) are obtained from the observed counts in detectors 6–9 (*left column*). The 'normalized residuals' are defined by $(c - \lambda)/\sqrt{\lambda}$, with λ the predicted count rates (Equation (2)). Not all counts are shown.

the spin axis predicts periodicity for subcollimator 9 during almost the whole flare, and for subcollimators 6–9 during more than one minute at peak time. In fact, with the choice $\Delta t = 0.19$ ms, Equation (1) becomes $(0.005, 0.003, 0.002, 0.001) < 0.03\, a_0^i$ for subcollimators $i = (6,7,8,9)$ in the time interval 09:57:08–09:58:30 UT. The RHESSI spin period, obtained from a linear fit to the aspect solution $\Phi(t)$, is 4.334 s. The observed counts, corrected for lifetime, are shown in the left column, with the demodulated 'impulsive' contribution at the top left panel. The retrieved functions m^i, which are a proxy for the modulation functions, are presented in the middle column. The retrieved background (not shown) is approximately proportional to m, in agreement with the fact that CLEAN imaging (Högbom, 1974; Lannes, Anterrieu, and Maréchal, 1997) indicates the presence of a single source (same energy band; several 8 s-subintervals). The background contributes about 12 counts^{-1} Δt^{-1} subcollimator^{-1}; it is constrained by $\gamma = 0.2N/(N_S N_c \ln \bar{c})$. Diminishment of γ has a negligible effect on the solution (r, m, b). The final reduced log likelihood is -0.505, corresponding to reduced chi squares of (1.1, 0.96, 0.98,0.95) in subcollimators (6,7,8,9). The iterative convergence of the different terms of Equation (3) is shown in the top right panel, where all quantities are again normalized by the number of valid count rates. It can be seen that the trade-off is dominated by the likelihood, in the sense that the absolute change of $\ln L$ is larger than the absolute changes of A, B and C. (The change of $\ln L$ is more indicative than $\ln L$ itself, because $\ln L$ contains summands which are independent of (r, m, b).) The dominance of $\ln L$ suggests that the qualitative features of the solution (r, m, b) are determined by the agreement between prediction and observation rather than by the regularization.

Another example flare event was observed at 11:06 UT of the same date as the previous example (Figure 4). The energy band is 12–50 keV. Here, the stability of the spin axis predicts periodicity only for the coarsest subcollimators. The time bin size is 8 ms, and the final reduced log likelihood is -0.507. The retrieved time profile (Figure 4, top) exhibits several features on time scale < 4 s; among which the peak at 11:06:44 UT is believed to be real, since it clearly correlates with a type III burst observed by the *Phoenix-2* radiometer (Messmer, Benz, and Monstein 1999) at ~ 600 MHz. The three 'peaks' at 11:06:14–24 UT might correspond to similar type III events, but are probably also contaminated by spurious spin periodicity which is not completely removed by the demodulation procedure. Contrary to the 09:58 UT flare event, the retrieved background was found to be nonproportional to the retrieved m, which is a hint to the presence of multiple sources. More precisely, the data are not compatible with the assumption that the X-ray brightness distribution is of the form $B(\mathbf{x}, t) = s(t) B_1(\mathbf{x})$. This rules out, for instance, a single time-dependent footpoint of a magnetic loop, or a pair of simultaneously flashing footpoints. Instead, there must be a further (temporally) independent component, which is likely to be driven by different physical causes or configurations.

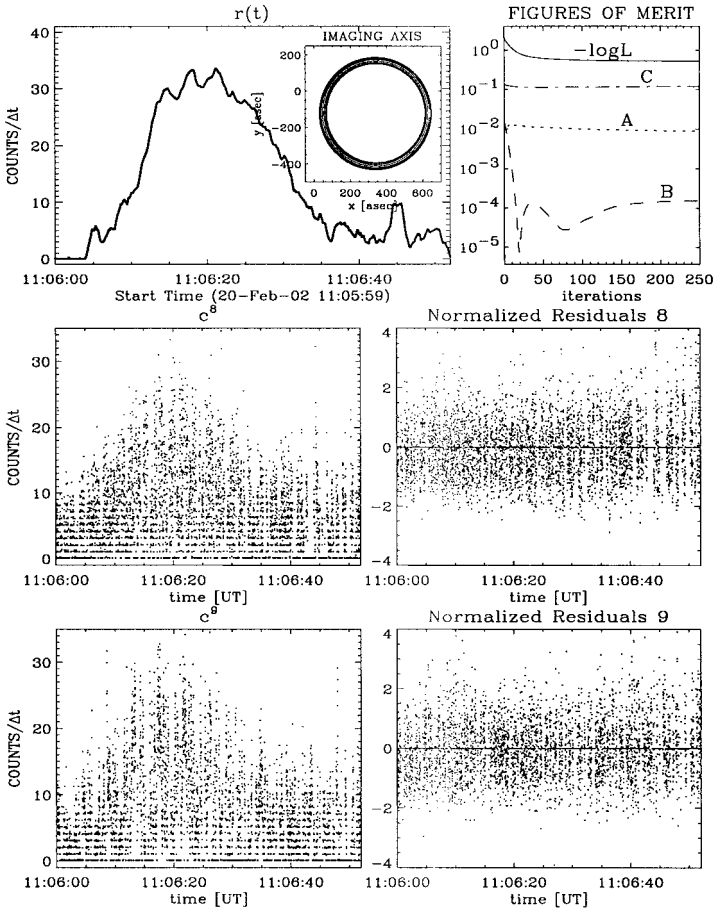

Figure 4. Demodulation of the flare of 20 February 2002, 11:06 UT in the energy band 12–50 keV, with $\Delta t = 8$ ms and $\tau = 0.25$ s. All observed counts in subcollimators 8 and 9 (*left column*) are shown.

A third example is provided by the flare of 17 March, 19:28 UT (Figure 5). Here, the energy band is 25–100 keV, and the background is neglected (frozen in). The comparably slow modulation indicates that the source(s) are close to the imaging axis. This, together with a good spin stability, admits the use of subcollimators, 4–9 over the time interval 19:27:25–19:29:10 UT, with $\Delta t = 0.19$ ms and $\tau = 0.25$ s. Subcollimator 5 is excluded, since it gives rise to spurious spin periodicity and an unsatisfactory likelihood ratio. This might be connected to known problems of this subcollimator, which could enter the demodulation through a wrong theoretical mean grid transmission. The retrieved 'impulsive' time profile shows several interesting short-scale features. The retrieved functions m bear close resemblance with the expected modulation functions, suggesting that the source(s) have not been resolved, except for possibly subcollimator 4. In fact, imaging reveals the presence

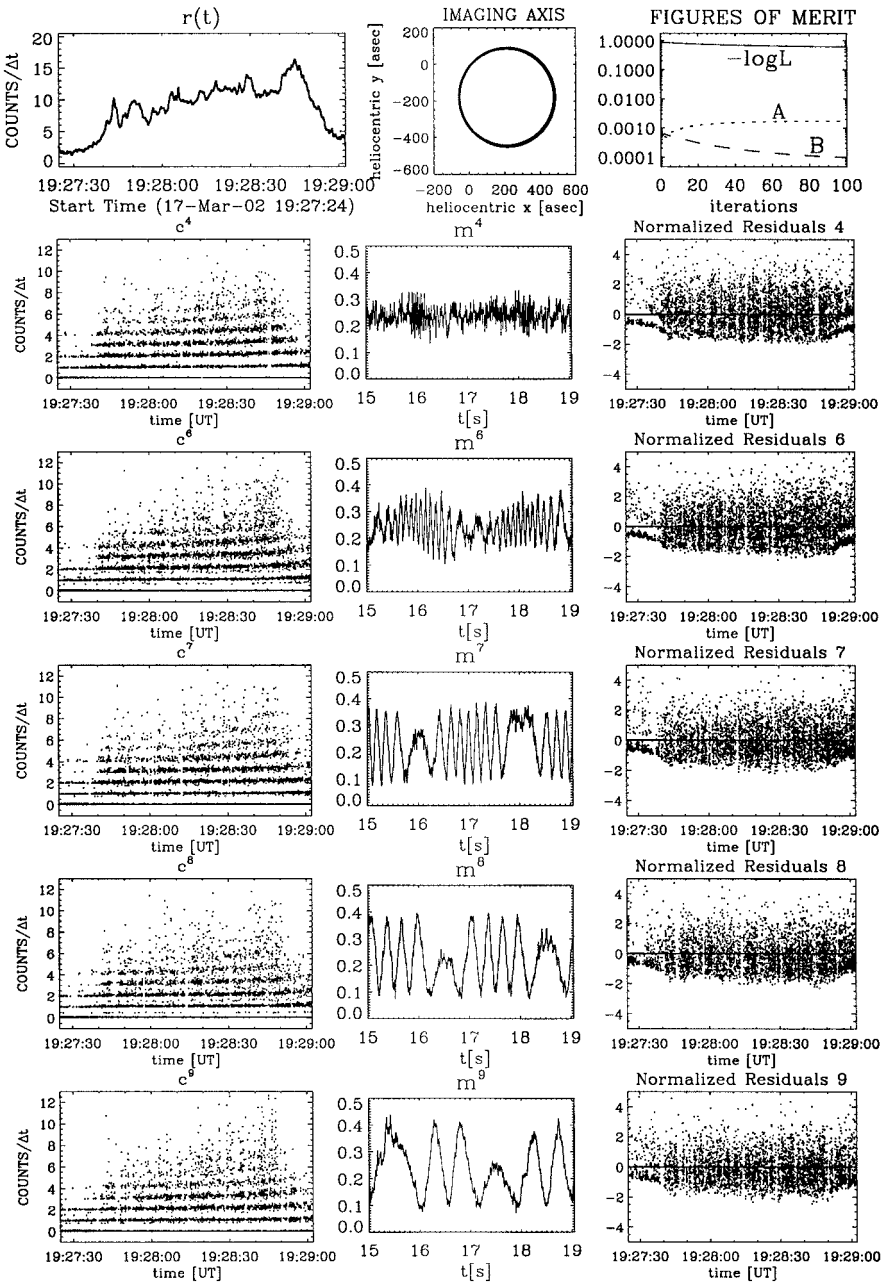

Figure 5. The flare of 17 March. 19:28 UT in the energy band 25–100 keV, with $\Delta t = 1.9$ ms and $\tau = 0.25$ s. Here, the background degrees of freedom are frozen in, thus assuming only contributions form the 'impulsive' source. Not all counts are shown.

of two or three sources within 20″, which makes the neglect of the background ($B(\mathbf{x}, t) = s(t)B_1(\mathbf{x})$) questionable for subcollimator 4 ($p^4 = 23''$). Note also the skewness of the residual ($(c - mr)/\sqrt{mr}$) distribution (right column), indicating that a normal approximation would not apply to the low count rates under consideration.

6. Summary and Discussion

A time-domain demodulation algorithm is developed and applied to RHESSI light curves, based on the simple observation that the count rates with comparable aspect data should coincide if the source distribution did not change with time. This allows to decompose the count rates into periodic and non-periodic contributions, where the periodic parts are due to modulation and background, and the non-periodic part represents the true time profile of an impulsive source. (Remember that 'periodic' includes the constant case.)

A thorough error analysis of the demodulated light curve $r(t)$ is not elementary and out of the scope of the present article. As an order-of-magnitude estimate, one may however argue as follows. By construction, $r(t)$ has correlation time τ, so that $\{r_t\}$, $t_0 \leq t \leq t_0 + \tau/\Delta t$, represents one degree of freedom. By coherently perturbing r_t in intervals of duration $\tau/\Delta t$ one can find that perturbation Δr which causes the (non-reduced) log likelihood, in average, to change by unity. This corresponds to a change of about 2 in the (non-reduced) chi square ($\sim 95\%$ confidence). For the flare of 20 February, 2002, 09:58 UT (Figure 3) one obtains $\Delta r_t \simeq 1.25$; for the flare of 20 February 2002, 11:06 UT (Figure 4) one finds $\Delta r \simeq 1.5$, and for the flare of 17 March 2002, 19:28 UT (Figure 5) $\Delta r \simeq 0.2$. The above estimates neglect other than Poisson errors, as well as errors due to m and b. The latter are not independent of r, but better known than r if several spin periods available. In practice, the reliability of r should always be verified by comparison with the observed counts, and by exploring different time intervals and sets of subcollimators.

Besides an intrinsic physical interest in short-time structures, the demodulation may also have implications for imaging, since it allows to verify (or disprove) the stationarity assumption underlying the current imaging algorithms. As a side product, it provides an independent estimate on the modulation functions, whenever the source is well-resolved ($m_t^i \simeq M^i(t)$), which is the case if the m_t^i covers the full theoretical range of $M^i(t)$.

The basic advantage of the presented demodulation method is its weak assumptions, which are likely to fail only if several 'impulsive' sources are present at the same time. Its principal limitation is the required aspect recurrence, which rules out the finest subcollimators. The recurrence condition (1) may be relaxed if the grid periodicity is taken into account, so that comparable times $\{t\}$ may occur at integer multiples of $T_S/2$ if $(\mathbf{k} \cdot \Delta\mathbf{P})/2\pi \simeq 0, \pm 1, \pm 2, \ldots$. This relaxation will

enlarge the set of flares which are amenable to the demodulation method. The finest subcollimators may be included in another way, e.g., by Wiener filtering. A consistent incorporation into the present framework is one of the major future projects, together with imposing a (computationally more expensive) non-periodicity constraint on r, instead of merely asking for smoothness. This is hoped to cure the spurious spin periodicity which is sometimes present in the demodulation. A – more theoretical – caveat is the use of Poisson statistics which is not properly defined for the non-stationary case. The Poisson assumption in Equation (3) is with the understanding that is represents a convenient and sensible approximation to the underlying binomial statistics.

Acknowledgements

The author thanks A. Benz, G. Hurford, R. Schwartz, A. Zehnder, and M. Fivian for helpful discussions and A. Benz for providing synoptic radio data.

Appendix
Existence of a Global Maximum of F

Here are some analytical arguments on the extremal problem $F = \max!$. A sufficient condition for a unique solution is the (strict) convexity of F. Let $x \doteq (r, m, b)$ and $F(x)$ be defined as in Equation (3). Remember that all elements of x are positive, and that $0 < m < 1$. Applying the triangle inequality to the sums over spin periods and subcollimators it can be shown that the Hessian $H_{ij} = \partial^2 F/\partial x_i \partial x_j$ satisfies $H_{ii} < 0$ and $H_{ii} H_{jj} > |H_{ij}|^2$, which is a necessary condition for negative definiticity. In order to characterise a sufficient condition, consider the function $\Delta F \doteq F(\frac{1}{2}(x_1 + x_2)) - \frac{1}{2}(F(x_1) + F(x_2))$. The discussion is restricted to a single subcollimator, since the inclusion of several subcollimators is not expected to degrade the conditioning. Convexity requires $\Delta F > 0$. Itemized by (r, m, b), one has that

$$\Delta F = \tfrac{1}{4}\sum(m_1 - m_2)(r_1 - r_2) + \tfrac{\alpha}{8}\sum(r_1 - r_2)\mathcal{D}(r_1 - r_2) + \\ + \tfrac{\beta}{8}(\sum(m_1 - m_2))^2 + \sum c \ln \tfrac{(b_1+b_2)/2+(m_1+m_2)(r_1+r_2)/4}{(b_1+m_1 r_1)^{1/2}(b_2+m_2 r_2)^{1/2}} + \gamma \sum \ln \tfrac{(b_1+b_2)/2}{(b_1 b_2)^{1/2}},$$

with $\mathcal{D}_{ij} = -\delta_{i-1,j} + 2\delta_{i,j} + \delta_{i+1,j}$ the 2nd order difference operator, and where the sums run over the full index sets. The 2nd, 3rd and 5th term of ΔF are non-negative definite (by positivity of $\mathcal{D}$ and β, and the arithmetic-geometric inequality), while the 1st and 4th term may be negative. Assume now that b is frozen to zero ($b_1 = b_2 \to 0$). The 5th term of ΔF then vanishes, and each summand of the 4th term possesses the (weak) lower bound

$$c \ln \tfrac{(m_1+m_2)(r_1+r_2)/4}{(m_1 r_1)^{1/2}(m_2 r_2)^{1/2}} = -\tfrac{1}{2} c \ln[1 - (\tfrac{m_1-m_2}{m_1+m_2})^2] - \tfrac{1}{2} c \ln[1 - (\tfrac{r_1-r_2}{r_1+r_2})^2] \geq \\ \geq \tfrac{1}{2} c (\tfrac{m_1-m_2}{m_1+m_2})^2 + \tfrac{1}{2} c (\tfrac{r_1-r_2}{r_1+r_2})^2 \geq \tfrac{1}{8} c (m_1 - m_2)^2 + \tfrac{1}{8 \max(r)^2} c (r_1 - r_2)^2,$$

where it was used that $-\ln(1-\xi) \geq \xi$ for $0 \leq \xi \leq 1$, and that $\max(m) < 1$. Therefore, $\Delta F \geq \frac{1}{4}(\Delta r, \Delta m)^T M(\Delta r, \Delta m)$, where the symmetric matrix $M = \begin{pmatrix} M^{rr} & M^{rm} \\ M^{mr} & M^{mm} \end{pmatrix}$ has the blocks $M_{ij}^{rr} = \frac{c_i}{\max(r)^2}\delta_{ij} + \alpha \mathcal{D}_{ij}$, $M_{ij}^{rm} = \delta_{i \bmod P, j}$, and $M_{ij}^{mm} = \delta_{ij} \sum_k c_{j+Pk} + \beta$. It may (numerically) be shown that M is positive definite for suitable $\alpha, \beta > 0$; increasing count rates favour the dominance of the diagonal blocks over the off-diagonal blocks, and allow decreasing regularization. The case $b_1 \neq b_2 > 0$ can be treated by similar lower bounds on the 4th and 5th terms of ΔF. Analytical regularity bounds on (α, β, γ), which are both rigorous and tight, were not obtained so far.

References

Benz, A. O. *et al.*: 1994, *Solar Phys.* **153**, 33.

Cash, W.: 1979, *Astrophys. J.* **228**, 939.

Dennis, B.: 1985, *Solar Phys.* **100**, 465.

Eadie, W. T., Drijard, D., James, F. E., Roos, M., Sadoulet, B.: 1971, *Statistical Methods in Experimental Physics*, Elsevier Science Publ., Amsterdam.

Fivian M., Hemmeck, R., Mchedlishvili, A., and Zehnder, A.: 2002, *Solar Phys.*, this volume.

Gary, D.: 2000, in R. Ramaty and N. Mandzhavidze (eds.), *High Energy Solar Physics – Anticipating HESSI, ASP Conference Series* **206**, 297.

Högbom, J. A.: 1974; *Astron. Astrophys. Suppl. Series* **15**, 417.

Hurford, G. J. and Curtis, D.: 2002, *Solar Phys.*, this volume.

Hurford G. J. *et al.*: 2002, *Solar Phys.*, this volume.

Kailath, T.: 1974, A view of three decades of linear filtering theory, *IEEE Trans. Info. Theory*, **IT-20**, 146.

Kane, S. R., Chupp, E. L., Forrest, D. E., Share, G., and Rieger, E.: 1986, *Astrophys. J.* **300**, L95.

Kiplinger, A. L., Dennis, B. R., Frost, K. J., and Orwig, L. E.: 1984, *Astrophys. J.* **28**, L105.

Lannes, A., Anterrieu, E., and Maréchal, P.: 1997, *Astron. Astrophys. Suppl. Ser.* **123**, 183.

Machado, M. E., Ong, K., Emslie, A. G., Fishman, G. J., Meegan, C., Wilson, R., and Paciesas, W. S.: 1993, *Adv. Space Res.* **13**, 175.

Mallat, S., 1998, *A wavelet tour of signal processing*, Academic Press, London.

Messmer, P., Benz, A. O., and Monstein, C.: 1999, *Solar Phys.* **187**, 335.

Miller, J. A., Ramaty, R., and Murphy, R. J.: 1987, *Proc. 20th Cosmic Rays Conf.* **3**, 33.

Miller, J. A., Cargill, P. J., Emslie, A. G., Holman, G. D., Dennis, B. R., LaRosa, T. N., Winglee, R. M., Benka, S. G., and Tsuneta, S.: 1997, *J. Geophys. Res.* **102**, 14 631.

Nakajima, H.: 2000, in R. Ramaty and N. Mandzhavidze (eds.), *ASP Conference Series* **206**, 313.

Press, W., Teukolsky, S., Vetterling, W., and Flannery, B.: 1998, *Numerical Recipes in C*, 2nd ed., Cambridge University Press, Cambridge.

Rosen, Y. and Porat, B.: 1989, *IEEE Trans. Info. Theory* **IT-35**, 342.

Schwartz, R. *et al.*: 2002, *Solar Phys.*, this volume.

Smith, D.: 2002, *Solar Phys.*, this volume.

Vautard, R. and Ghil, M.: 1989, *Physica* **D35**, 395.

Varadi F., Pap, J. M., Ulrich, R. K., Bertello, L., and Henney, C. J.: 1999, *Astrophys. J.* **526**, 1052.

Varadi F., Ulrich, R. K., Bertello, L., and Henney, C. J.: 2000, *Astrophys. J.* **526**, L53.